



# Atmospheric dynamics of extreme discharge events from 1979 to 2016 in the southern Central Andes

F. Castino<sup>1</sup> · B. Bookhagen<sup>1</sup> · A. de la Torre<sup>2</sup>

Received: 22 December 2019 / Accepted: 8 September 2020 / Published online: 16 September 2020  
© The Author(s) 2020

## Abstract

During the South-American Monsoon season, deep convective systems occur at the eastern flank of the Central Andes leading to heavy rainfall and flooding. We investigate the large- and meso-scale atmospheric dynamics associated with extreme discharge events (> 99.9th percentile) observed in two major river catchments meridionally stretching from humid to semi-arid conditions in the southern Central Andes. Based on daily gauge time series and ERA-Interim reanalysis, we made the following three key observations: (1) for the period 1940–2016 daily discharge exhibits more pronounced variability in the southern, semi-arid than in the northern, humid catchments. This is due to a smaller ratio of discharge magnitudes between intermediate (0.2 year return period) and rare events (20 year return period) in the semi-arid compared to the humid areas; (2) The climatological composites of the 40 largest discharge events showed characteristic atmospheric features of cold surges based on 5-day time-lagged sequences of geopotential height at different levels in the troposphere; (3) A subjective classification revealed that 80% of the 40 largest discharge events are mainly associated with the north-northeastward migration of frontal systems and 2/3 of these are cold fronts, i.e. cold surges. This work highlights the importance of cold surges and their related atmospheric processes for the generation of heavy rainfall events and floods in the southern Central Andes.

**Keywords** South American monsoon system · Cold surges · Orographic barrier · Mesoscale convective systems · Extreme discharge · Daily-discharge time series ERA-interim

## 1 Introduction

In high-mountain regions strong convective events lead to high discharge often resulting in floods that critically impact local infrastructures and landscape causing economic and population losses (Wolman and Miller 1960; Plate 2002). This is particularly true for the intermediate elevations of the eastern Central Andes that are exposed to the South American Monsoon System (SAMS) (Zhou and Lau 1998; Vera et al. 2006; Silva and Carvalho 2007; Marengo et al. 2012).

The intermontane basins of northwestern Argentina constitute part of the Andean tributaries of the La Plata River, the second largest river basin in South America that flows across one of the most populated and economically relevant areas of the continent. In this region, heavy discharge events repeatedly flood agricultural fields and increase demand of infrastructural maintenance (Marcato et al. 2009, 2012; de la Torre et al. 2011).

A previous study based on gauge data for the period from 1940 to present (Castino et al. 2017b) suggested that a significant fraction of the multi-annual to multi-decadal variability of river discharge in this region is linked to large-scale ocean–atmosphere coupled processes, for example expressed as the Tropical South-Atlantic sea surface temperature anomaly (Enfield and Mestas-Nunez 1999) and the Pacific Decadal Oscillation (PDO) (Mantua and Hare 2002). Castino et al. (2017a, b) also documented a steady intensification of the hydrological cycle—both in rainfall and river discharge—in the past decades (1940 to present) for this region. This intensification has been pronounced for the uppermost percentiles (> 95th) of the frequency

---

**Electronic supplementary material** The online version of this article (<https://doi.org/10.1007/s00382-020-05458-1>) contains supplementary material, which is available to authorized users.

---

✉ F. Castino  
castino@uni-potsdam.de

<sup>1</sup> Institute of Geosciences, University of Potsdam, Potsdam, Germany

<sup>2</sup> Faculty of Engineering, LIDTUA, Austral University and CONICET, Pilar, Buenos Aires, Argentina

distributions of daily observations, suggesting larger rates of change for extreme hydro-meteorological events in these montane catchments. Similar results have been observed for northeastern Argentina, showing an increase in intense precipitation starting in 1970 (Lovino et al. 2018). Segura et al. (2020) have also observed the intensification of the precipitation over the southern tropical Andes ( $12^{\circ}$ – $20^{\circ}$  S,  $> 3000$  m asl) in the period 1982–2017, linking it to the strengthening of the upward motion (i.e., convection) over the western Amazon.

Boers et al. (2014, 2015) attempted to identify the event-scale causes of extreme hydro-meteorological events ( $> 99$ th percentile) in the eastern flank of the Central Andes using the satellite-derived and gauge-calibrated rainfall dataset TRMM 3B42V7 (Huffman et al. 2007). These authors showed that extremes at the eastern flank of the southern Central Andes originate from frontal systems moving northward from the central Argentinean plains. Boers et al. (2014) showed that more than 60% of these extreme events are associated with preceding extreme rainfall (within 2 days) in the region of South-East South America (SESA) and a low pressure anomaly in north-western (NW) Argentina. These authors associated the northward migration of a frontal system with cold surges, one of the major climate features affecting South American rainfall patterns, particularly during the wet season (e.g., Marengo et al. 1997; Garreaud and Wallace 1998; Garreaud 2000; Lupo et al. 2001; Vera and Vigliarolo 2002; Espinoza et al. 2012; Rasmussen and Houze 2016; Sicart et al. 2016; Paccini et al. 2018; Prince and Evans 2018). While their study identifies the spatiotemporal correlation between rainfall events in SESA and the eastern Central Andes, they do not analyze the atmospheric dynamics leading to these events.

At continental scale, other studies attempted to link extreme rainfall events in South America with atmospheric features controlled by the South American Low-Level Jet (SALLJ) and the South Atlantic Convergence Zone (SACZ), or with climate modes of variability such as the El Niño Southern Oscillation (ENSO) (e.g., Marengo et al. 1998, 2004; Carvalho et al. 2002, 2012; Vera et al. 2006). At more regional scale, several studies have shown that intense rainfall along the eastern flank of the Central Andes both in the tropical and subtropical parts are mainly associated with mesoscale convective systems (MCSs). These MCSs are triggered by orographic uplift or atmospheric instability and often form locally and propagate to the eastern flanks of the Central Andes (Maddox et al. 1979; Cohen et al. 1995; Garreaud 2000; Durkee et al. 2009; Romatschke and Houze 2013). Espinoza et al. (2015) have identified rainfall hotspots at low elevations in the Andean foothills of Peru and Bolivia. They have shown that rainfall maxima are controlled by the geometry and orientation of the mountain range to the atmospheric circulation, with observed precipitation peaks

up to 6 m/year. It has been documented that in Bolivia the frequency of extreme rainfall events increases during the positive phase of the PDO, whereas drier conditions in the Bolivian Andes occur during the positive phase of ENSO (Seiler et al. 2013; Sulca et al. 2018; Segura et al. 2019). Perry et al. (2014) have observed that different regions contribute to low-level moisture for precipitation events in the tropical Andes of southern Peru. These authors evidenced that more than 80% of precipitation events are dominated by weak flow regimes from the nearby Amazon basin and 50% are associated with northwesterly flows (SALLJ). In addition, Hurley et al. (2015) analyzed 10 years of hourly snow-height measurements at the summit of the Quelccaya Ice Cap (southeastern Peruvian Andes), where the oldest and most precisely dated high-resolution paleoclimate record from the tropical Andes has been collected (Thompson et al. 1985). These authors showed that in this area more than 70% of the annual snow accumulation occurs in association with convection along the leading edge of mid-latitude cold air incursions advected equatorward from southern South America (cold surges).

This study focuses on the eastern flank of the southern Central Andes, at the end of the conveyor belt of the SALLJ in the transition to the extratropical region. In this area, at least to the knowledge of the authors, no study investigated the atmospheric dynamics associated with extreme hydro-meteorological events. Few recent studies have showed relevant changes in the atmospheric circulation over the Amazon basin, which also affected the precipitation pattern, with intensified (decreased) rainfall in northern (southern) Amazon starting by the end of the twentieth century (Barichivich et al. 2018; Wang et al. 2018; Espinoza et al. 2019). These changes in the atmospheric circulation over the Amazon basin have been also linked to the intensification of precipitation in the southern tropical Andes (Segura et al. 2020). A better knowledge of the large- and meso-scale atmospheric processes that trigger extreme discharge event in the southern Central Andes is crucial not only to understand present-day variability of the precipitation pattern, but also to correctly interpret past climate records (Luna et al. 2018) and to understand and predict future climate change.

The present study aims at deciphering the meso- to synoptic-scale atmospheric patterns leading to hydro-meteorological events in the southern Central Andes of NW Argentina in the past four decades (1979–2016). The focus is to identify the atmospheric conditions of the 40 strongest discharge events (99.9th percentile) based on eleven daily rainfall and seven river-discharge time series from gauge stations. The station data are combined with ERA-Interim reanalysis provided by the European Centre for Medium-Range Weather Forecast (ECMWF) for the period from 1979 to 2016. The gauge data of the mountainous catchments provide important constraints on the

hydro-meteorologic variability and integrate catchment-scale precipitation for ~76 years (1940–2016) that allow to measure their dynamic range and magnitude-frequency distribution. Based on these datasets, we present an analysis of the rank-ordered magnitude-frequency relation of the discharge and focus on extreme events (>99.9th percentile) during the past ~30 years. In a second step, we identify the atmospheric conditions leading to extreme events by focusing on different atmospheric variables including total water content, air temperature, specific humidity, and wind speed and direction at the surface and at different height levels.

## 2 Geographic and climatic setting

The 7000 km long, meridionally-oriented Andean orogen with elevations between 5 and 7 km asl forms a hemispheric-scale orographic barrier for atmospheric circulation systems

(Fig. 1a). The study area is located between 21° and 28° S in the southern Central Andes in NW Argentina. It comprises the low elevations to the east of the Andes at about 500 m asl, the steep eastern Andean flanks, and the high-elevation region of the southern Central Andes with peaks in excess of 6 km elevation (Fig. 1a). The interaction between topography and the hemispheric-scale atmospheric circulation controls the rainfall pattern in the southern Central Andes (Gandu and Geisler 1991; Campetella and Vera 2002; Bookhagen and Strecker 2008; Gabet et al. 2008; Garreaud et al. 2010). Moisture transport into this region is driven by the SAMS from September to April (Zhou and Lau 1998; Vera et al. 2006; Silva and Carvalho 2007; Marengo et al. 2012). During the monsoon season, moisture from the tropical Atlantic Ocean is partly released in form of intense rainfall at the eastern flank of the tropical Andes and partly advected southward towards the subtropical areas of South America. Important features controlling the southward advection of moisture are the SALLJ and the SACZ (Gandu

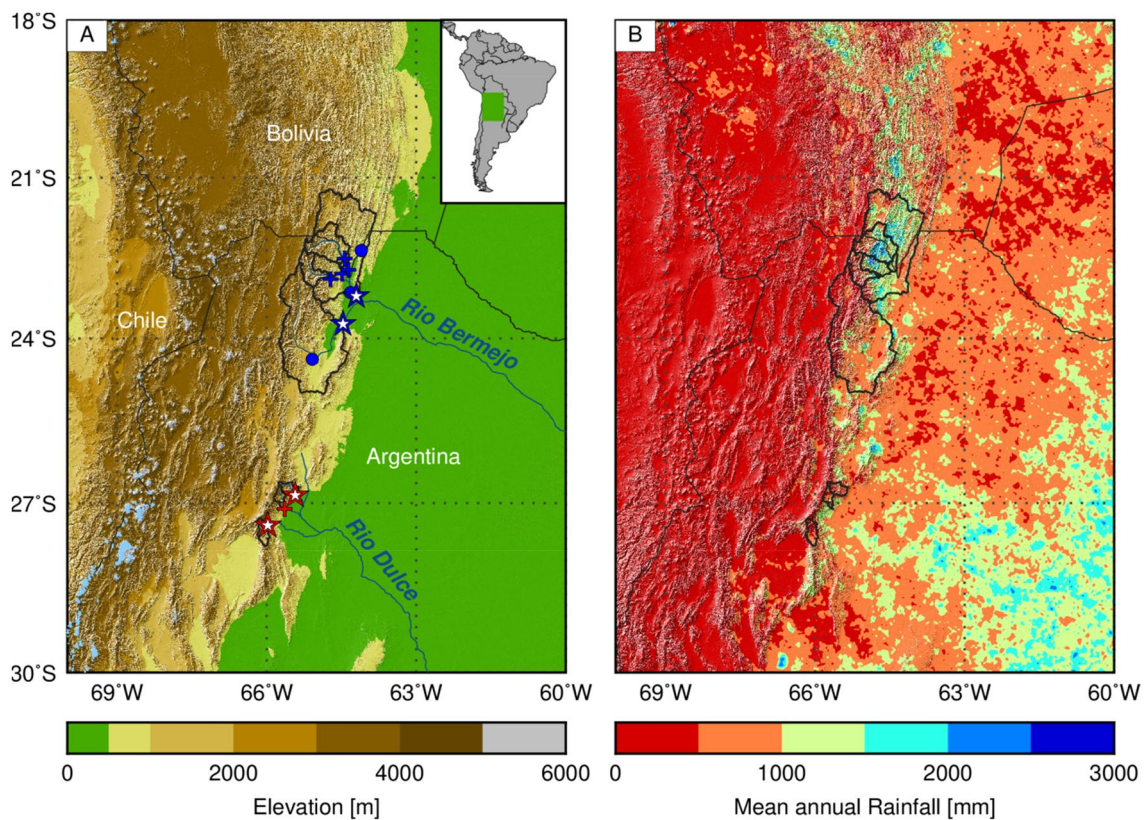


**Fig. 1** **a** Topography (SRTM) of the southern Central Andes showing the location of gauge stations (circles refer to rainfall-only stations, crosses indicate discharge and rainfall stations) for the humid Upper Rio Bermejo (blue) and semi-arid Rio Dulce (red) drainage basins. Stars indicate the catchment-representative stations used for the analysis from each main catchment. Black polygons represent the drained area at the discharge station locations. The Randolph Glacier Inventory V6 (RGI-Consortium 2017) has been used for glaciers outlines

(light blue); the thin dark grey line denotes international borders. The green rectangle in the inset indicates the study area. **b** Mean annual rainfall derived from TRMM 2B31 V7 (1998–2014) (Bookhagen and Strecker 2008; Bookhagen and Burbank 2010) showing a pronounced gradient between low-elevation frontal areas (>2000 mm/year) and arid, high-elevation areas of the orogen interior (<500 mm/year) resulting in a highly climatic heterogeneity ranging from humid to semi-arid conditions (Castino et al. 2016, 2017a)

and Silva Dias 1998; Vera et al. 2006; Marengo et al. 2012; Boers et al. 2015).

More than 80% of the annual precipitation in the eastern flanks of the NW Argentine Andes falls during the wet season, between November and March (Rohmeder 1943; Halloy 1982; Bianchi and Yañez 1992; Garreaud et al. 2003, 2010; Castino et al. 2017a). The distribution of rainfall maxima at the windward flanks of the subtropical Central Andes is controlled by the geometry of the mountain range with significant orographic rainfall peaks (Seluchi and Marengo 2000; Bookhagen and Strecker 2008; Giovannettone and Barros 2009; Espinoza et al. 2015). Mesoscale convective systems (MCSs), forming locally and triggered by orographic uplift or atmospheric instability, are the primary source of intense rainfall events both in the tropical and subtropical parts of the Andean mountain range (Maddox et al. 1979; Garreaud 2000; Romatschke and Houze 2013; Boers et al. 2015).

On interannual timescales, the rainfall patterns in the NW Argentine Andes are modulated by the interplay between different atmospheric features, such as the Bolivian High, the Chaco Low, and the North-Western Argentinian Low (Schwerdtfeger 1976; Gandu and Silva Dias 1998; Salio et al. 2002; Seluchi et al. 2003; Carvalho et al. 2004; Vuille and Keimig 2004; Boers et al. 2014). In addition, different climate disturbances, such as the Madden–Julian Oscillation, the ENSO or the PDO, substantially affect the overall rainfall pattern during the SAMS, especially by controlling the strength of the SALLJ and SACZ (Madden and Julian 1971; Vuille et al. 2000; Garreaud and Aceituno 2001; Mantua and Hare 2002; Castino et al. 2017b). These changes often result in increased precipitation in the higher elevation, semi-arid to arid regions of the orogen interior, which leads to increased runoff, erosion, and deposition in the intermontane basins (Strecker et al. 2007; Bookhagen and Strecker 2012).

In the southern Central Andes, the pronounced rainfall seasonality is reflected by the annual cycle of river discharge in intermontane catchments, exhibiting homogeneous unimodal hydrographs with peak-discharge values between February and March (Pasquini and Depetris 2007; Castino et al. 2016) (Fig. S1, Supplementary material). Major river catchments originating in this region are the Rio Bermejo ( $123 \times 10^3$  km<sup>2</sup> catchment size, 1060 km length, measured to the confluence with the Rio Paraná), and the Rio Dulce [ $90 \times 10^3$  km<sup>2</sup> catchment size, 810 km length, measured to the outlet into the Laguna Mar Chiquita, the largest Argentine salt lake (SSRH 2004)] (Fig. 1a). Importantly, in contrast to the tropical Andes to the north and the southern Andes, there are currently no glaciated peaks in this region (Lliboutry 1998) (Fig. 1A), resulting in a negligible contribution to streamflow from snow- and ice-melt compared to rainfall (Bookhagen, 2016). Drainage basins in this area encompassing the intermontane valleys have small to medium-size catchments ( $10^2$ – $10^4$  km<sup>2</sup>), with headwaters

located at elevations above 4 km asl, which results in steep river gradients (Bookhagen and Strecker 2012).

### 3 Data and methods

In this study we used two different datasets: hydro-meteorological ground-station observations and reanalysis data at different height levels. We considered two time periods: from 1940 to 2016 covering the availability of the ground-station data, and from 1979 to 2016 covering the reanalysis dataset.

#### 3.1 Ground-station observations

The hydrologic-station data contain daily time series from nine gauge stations measuring both river discharge and rainfall and two other stations measuring only rainfall (Fig. 1a and Supplementary material). These stations are operated by the Argentine National Water Resources Agency (Subsecretaría de Recursos Hídricos) and the Argentine National Weather Service (Servicio Meteorológico Nacional) and are located in the Upper Rio Bermejo (six river discharge and rainfall and two rainfall-only stations) and Rio Dulce (three stations for rainfall and river discharge) catchments. It has been observed that river-discharge measurements are usually affected by uncertainties due to the instability of the river cross-section, in addition to those associated with the stage-discharge rating curve (Hersch 1978; Di Baldassarre and Montanari 2009). Although similar uncertainties may affect the precise quantification of the measurements error of the river-discharge dataset (see the Supplementary material for more details), this limitation has a relatively small impact on our study: First, we rely on the identification of the timing of the largest events and these are adequately recorded. Second, we identify the largest differences between humid and semi-arid discharge distributions to be of intermediate magnitudes, likely not strongly affected by measurements uncertainties.

The gauged drainage basins differ in climatic conditions from predominantly humid to semi-arid environments (Fig. 1b) but also in basin size ( $10^2$ – $10^4$  km<sup>2</sup>), with differences that are particularly pronounced between the Upper Rio Bermejo and the Rio Dulce catchments (Fig. 1b). In order to provide a reliable comparison between different climatic conditions, we performed our analysis using specific-discharge time series, calculated as the ratio of river discharge and catchment area at the station location (Castino et al. 2016). The quality of the dataset was tested using standard quality control checks (Rodda 2011; Antolini et al. 2015), showing a high degree of continuity and completeness (> 85%) for the period from 1979 to 2016 (Supplementary material, Table S1).

A preliminary analysis of the frequency distributions of the daily time series available for the period between 1940 and 2016 of specific discharge (seven time series) and rainfall (eleven time series) was performed for assessing their similarities and differences with specific focus on extreme and rare events. Subsequently, the daily observations of specific-river discharge were used to identify the largest 10 hydro-meteorological events (> 99.9th percentile, hereafter referred as extreme) for each gauge station that occurred between 1979 and 2016 in the study area. We focused our analysis on the period between November and April (NDJFMA), because on average this season contributes up to 90% to the total annual discharge (Fig. S1, Supplementary material). In this study, a hydro-meteorological event, or a *discharge event*, is defined as any monotonically increasing sequence of daily discharge observations with discharge-event duration and magnitude given by the length in days and the value of total increase of the discharge sequence, respectively (Fig. S2, Supplementary material). We selected the largest discharge events at daily timescales and we did not apply any filter for discarding minor discharge events that are small relative to the measuring error (Mutzner et al. 2013; Ye et al. 2014; Dralle et al. 2017). It was shown in a previous study that discharge time series within the same catchment are strongly correlated with lag-time between -1 and 1 day (Castino et al. 2016 and Fig. S3, Supplementary material). In addition, in the Upper Rio Bermejo catchment four out of six time series are from gauge stations in tributaries located upstream of the SA0693 gauge station. To decrease data redundancy without drastically reducing our ability of capturing a large portion of the local climate variability, our analysis was performed using two time series for each catchment, draining the upstream and downstream portion of the same drainage basin. The gauge stations SA0693 (downstream) and JU0016 (upstream) were used as catchment-representative stations for the Upper Rio Bermejo, whereas the gauge stations TU0411 (downstream) and TU0409 (upstream) were used as catchment-representative stations for the Rio Dulce. For each of these four stations the

time series of river discharge were analyzed for identifying the 10 largest events, resulting in a total of 40 events.

### 3.2 Reanalysis

We used the ERA-Interim reanalysis provided by the European Centre for Medium-Range Weather Forecasts (ECMWF) for the period from 1979 to 2016 with  $0.75^\circ \times 0.75^\circ$  spatial and 6-hourly temporal resolutions (Dee et al. 2011). The area considered for the analysis of the meso- and synoptic-scale atmospheric patterns includes South America and large portions of the South Pacific and Atlantic oceans ( $10^\circ\text{N}$ – $70^\circ\text{S}$ ,  $180^\circ\text{W}$ – $0^\circ$ ). We used two surface variables (total column water and 2 m air temperature) as well as four three-dimensional variables (geopotential height, temperature, wind speed and direction, and specific humidity) at different vertical levels from the surface up to the high troposphere (Table 1). The ERA-Interim reanalysis data have been used in many studies in several research fields, e.g., in climatology and hydro-meteorology and results suggest a high degree of reliability (Hodges et al. 2011; Mooney et al. 2011; Solman et al. 2013; Poveda et al. 2014; Boilley and Wald 2015).

The ERA-Interim dataset was used to analyze the large- and meso-scale atmospheric patterns and their dynamics during the extreme discharge events. We first estimated seasonal mean values for austral spring (SON), summer (DJF), and fall (MAM) for the period 1981–2010 for the surface and three-dimensional considered variables. These average values represent the climatology to which anomalies were evaluated.

To match the temporal resolution of the river-discharge observations, we analyzed daily full fields and anomalies from the ERA-Interim dataset. Compagnucci et al. (2001) suggested that the optimal time-sequence length for capturing the synoptic evolution of relevant weather systems in South America is 5 days. Thus, for each extreme discharge event we generated 5-day time-lagged sequences of both

**Table 1** Characteristics of ERA-Interim reanalysis and list of variables used in this study

Horizontal spatial resolution	$0.75^\circ \times 0.75^\circ$
Vertical levels	
Specific humidity and wind speed/direction	1000, 925, 850, 700, 500, 200 hPa
Geopotential height and air temperature	1000, 925, and every 50 hPa from 850 to 200 hPa
Time resolution	6 h
Surface variables	Total column water 2 m air temperature
Three-dimensional variables	Geopotential height Air temperature Wind speed and direction Specific humidity

mean daily full data and anomalies with respect to the seasonal climatology starting three days before and ending one day after each event (see Table 1 for a detailed description of the considered variables).

To analyze the average three-dimensional structure and evolution of the atmospheric patterns associated with extreme discharge events at large scales, we applied a standard time-lagged composite of surface and three-dimensional variables for full data and anomalies (Garreaud 2000; Rasmussen and Houze 2016). The significance of the anomaly values of the composites was tested using a standard Student's t-test at the 5% significance level. In addition, given that mesoscale atmospheric features may be averaged out by a compositing methodology, a subjective classification technique was applied for grouping extreme discharge events with similar dynamics of the mesoscale atmospheric patterns (Huth et al. 2008). Based on the 5-day time-lagged sequences derived from the ERA-Interim data, we visually analyzed the 850 hPa wind and specific humidity anomalies at mesoscale for classifying the dynamics of the atmospheric-circulation pattern associated with extreme discharge events in the study area (see the "Appendix" for details on the subjective classification).

## 4 Results

### 4.1 Ground-station observations

The frequency distribution of daily specific-discharge observations shows that differences in the intermediate events ( $Q_{0.2y}$ , 0.2 year mean return-period value, i.e. > 98th percentile) between gauge stations are almost as large as one order of magnitude, whereas rare events ( $Q_{20y}$ , 20 years mean return-period value, i.e. > 99.9th percentile) have smaller magnitude differences (Fig. 2a). The predominantly semi-arid catchment exhibits the largest ratio between rare and intermediate events magnitude ( $Q_{20\text{ years}}/Q_{0.2\text{ year}}$ ), in contrast with the predominantly humid catchment that shows the smallest ratio between rare and intermediate events magnitude. These differences in magnitude ratios between intermediate and rare (i.e., extreme) discharge events indicate heavier frequency-distribution tails for the semi-arid catchments than for the more humid ones. On the other hand, rainfall time series exhibit distributions with similar shape and scale independently of the overall hydroclimatic condition (either humid or semi-arid) of the catchment in which they are located (Fig. 2b).

The discharge-event analysis shows that more than half of the total discharge events for each time series have durations shorter than two days (Fig. S4, Supplementary material, only results from the catchment-representative stations are shown).

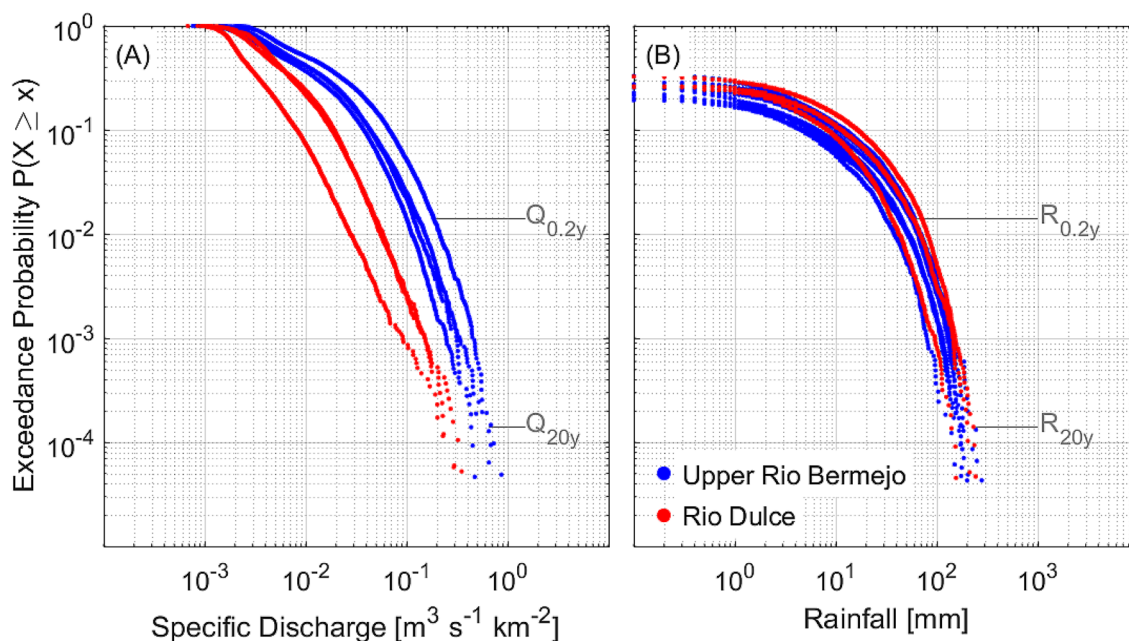


**Fig. 2** Exceedance probability plots for the period between 1940 and 2016 for the daily time series of **a** specific discharge (discharge normalized by the surface area of the corresponding catchment) and **b** rainfall from the gauge stations operating between 1940 and 2016 in the study area (Table S1, Supplementary material). Data from the

Upper Rio Bermejo (predominantly humid) and the Rio Dulce (predominantly semi-arid) are indicated with blue and red dots, respectively.  $X_{0.2y}$  and  $X_{20y}$ , with  $X=Q$  (specific discharge),  $R$  (rainfall), indicate the 0.2 year (intermediate event) and 20 years (rare event) mean return-period values, respectively

In addition, large events (discharge-event magnitude > 95th percentile) last less than seven days with less than 10% longer than 4 days (Fig. S5, Supplementary material). Taken together, the 10 largest discharge events (> 99.9th percentile) for each catchment (i.e., in total 40 events) contribute to more than 50% of the annual mean discharge (Table S2–3, Supplementary material).

## 4.2 Reanalysis data

### 4.2.1 Climatology of the large- and synoptic-scale atmospheric patterns

The composites of the time-lagged sequences show that on average between Day – 2 and Day – 1 a mid-level circulation with an eastward-migrating pressure dipole dominates the large-scale circulation over South America (Fig. 3, left panels). This pressure dipole has a moderate baroclinic character, as it is shown by the largely statistically significant 500 hPa geopotential-height anomaly (Fig. 3, left panels and Fig. S6, Supplementary material). Between Day – 1 and Day 0, the high pressure center of the dipole moves to the east of the Andean mountains, whereas the cyclone over the southwest Atlantic has reached its mature stage advecting relatively dry and cold air masses from higher latitudes into the continent. At low levels, a moderate low-pressure system associated with intense north-westerly winds occurs east of the Central Andes, whose intensity gradually decreases as the high-pressure system crosses the Andes by Day – 1 (Fig. 3, left panels). The composite maps of surface variables show a high water content in the atmosphere, combined with higher than normal surface air temperature (Fig. 3, right panel). Until Day 0, to the east of the southern Central Andes the air-temperature and water-content anomalies are particularly strong, condition also confirmed by its statistical significance (Fig. S6, Supplementary material), documenting the thermal character of the low-levels low-pressure system. When the high pressure cell crosses the Andes (between Day – 1 and 0), we observe a strong surface-level air temperature decrease that results in a negative temperature anomaly in the study area (Fig. 3, right panels, and Fig. S6, Supplementary material).

### 4.2.2 Mesoscale atmospheric patterns for extreme discharge events

In order to document the mesoscale dynamics features of the atmospheric patterns associated with extreme discharge events, we applied a subjective classification to the ERA-Interim data (see “Appendix” for details). Focusing on specific-humidity and wind anomalies, we identified three general groups with similar mesoscale dynamics (Table 2). We observe that Group 1 is almost equally constituted by events alternatively recorded by gauge stations in the Upper Rio

Bermejo and Rio Dulce. Group 2 is constituted mainly by events recorded in the Upper Rio Bermejo and occasionally affect also the Rio Dulce region, and Group 3 contains events mostly impacting the Rio Dulce. This grouping allowed us to describe 80% of all considered events (i.e., 32 out of 40 events). The rest can be roughly divided into either a weak, but continuous northerly wind flow (5%, 2 events) or a fast rotating wind flow from south to north before the event and from north to south after the event day (15%, 6 events). We generate composite maps for all events and for each group of events for describing the large-scale atmospheric dynamics associated with these discharge events (Figs. 3, 8). However, since such composite averages lead to a smoothing of the spatially-confined anomalies and an overall lower anomaly, we focus our analysis on three individual case studies that are representative of the main characteristics for each group.

Group 1 (15 events): The extreme event on February, 25th, 2010, largely affected the humid area of the Upper Rio Bermejo, but resulted in moderate discharge values also in the Rio Dulce. It was the third largest event between 1979 and 2016, with a peak discharge 22-times the annual average value (Table S2, Supplementary material, and Fig. 4, left panel). An intense north-westerly wind anomaly at low levels on the eastern flank of the Central Andes by Day – 3 was associated with a positive specific-humidity anomaly (Fig. 5, central panel). A high total column water is also observed over a broad area from the mountain to the eastern coast of the continent with a maximum located in SESA, accompanied by positive air temperature anomalies almost at every level, but particularly large at low levels in the east of the southern Central Andes (Fig. 5, left and right panels). On Day – 2 the warm and moist north-westerly flow intensified between 18° and 24° S, whereas a colder and drier southerly flow in the east of the Andes started to affect the region to the south of 30° S and partly converged with the northwesterly flow into an intense cyclonic flow over SESA. By Day – 1 the north-westerly flow weakened, the negative air-temperature anomaly shifted eastward and intensified reaching the northernmost region of the study area to the east of the Central Andes, accompanied by a large low-level humidity advection. This circulation pattern continued on Day 0, reaching its maximum moisture-flux anomaly in the northern region of the study area, still accompanied by a positive total-column water anomaly, while extending the low-level cold and dry anomaly to SESA. By Day 1 the dry and cold low-level core was established east of the Central Andes whereas the south-easterly flow started to weaken.

Group 2 (11 events): The representative event on January, 28–29th, 1979 has affected the Upper Rio Bermejo and the Rio Dulce river basins, resulting in the second largest event of the upstream portion of the Upper Rio Bermejo. It is associated with a peak-discharge value 20 times larger than the average annual discharge (Tables S2–3, Supplementary material, and

**Fig. 3** Climatological composites of the 5-day time-lagged sequences (from 3 days before to the day after the event) of ERA-Interim data for the 40 largest discharge events (> 99.9th percentile): (left column) 500 hPa and 850 hPa anomalies of geopotential height (GH) and 850 hPa anomalies of wind speed and direction (WS); shades and thick black isolines (every 10 m, solid for positive, dashed for negative values) indicate 850 hPa and 500 hPa GH, respectively, and arrows indicate WS; (right column) anomaly of total column water (TCW) and 2 m air temperature (2 m  $T_a$ ); shades and isolines (every 0.5°, red colors for positive, blue colors for negative anomalies) indicate TCW and 2 m  $T_a$ , respectively. Black stars and thin black isolines indicate the center of the study area and the terrain elevation (every 2000 m), respectively

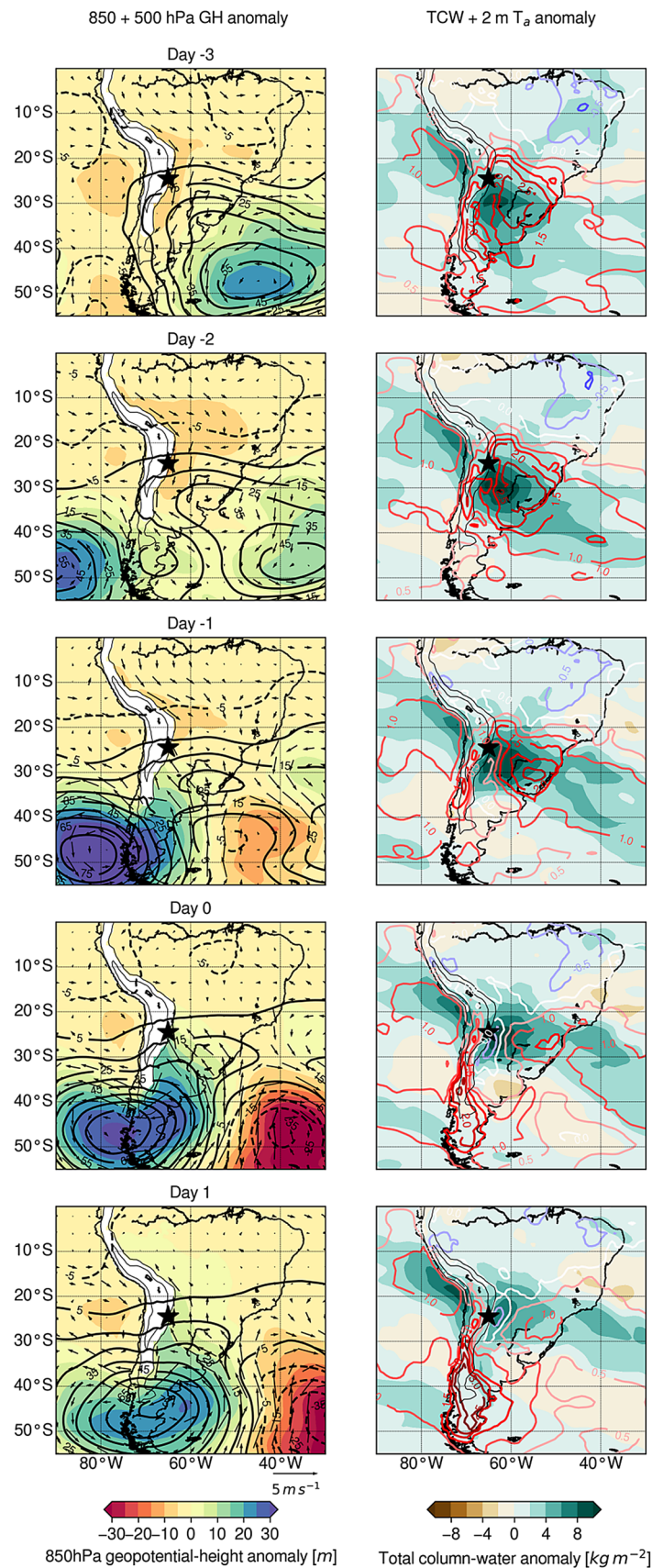




**Table 2** Main mesoscale features of the dynamics of atmospheric patterns associated with the three groups of the extreme discharge events (> 99.9th percentile)

Group	%	Wind and moisture-advection anomaly			
		Day - 3 and -2	Day - 1	Day 0 and 1	Affected areas
1	39	Intensifying northerly flow, strong moisture advection	Strong southerly flow, increasing moisture advection	Weakening of southerly flow and moisture advection	Alternatively Upper Rio Bermejo (extremely large discharge values) and Rio Dulce
2	25	Weak southerly flow, negligible moisture advection	Intensification of the southerly flow, strong moisture advection	Weakening of southerly flow and moisture advection	More frequently the Rio Bermejo, but occasionally also the Rio Dulce
3	14	Variable weak flow and low moisture advection	Intensified south-easterly flow with moderate moisture advection	Attenuation of the flow	Mostly Rio Dulce

% Indicates the percentage of events classified in each group

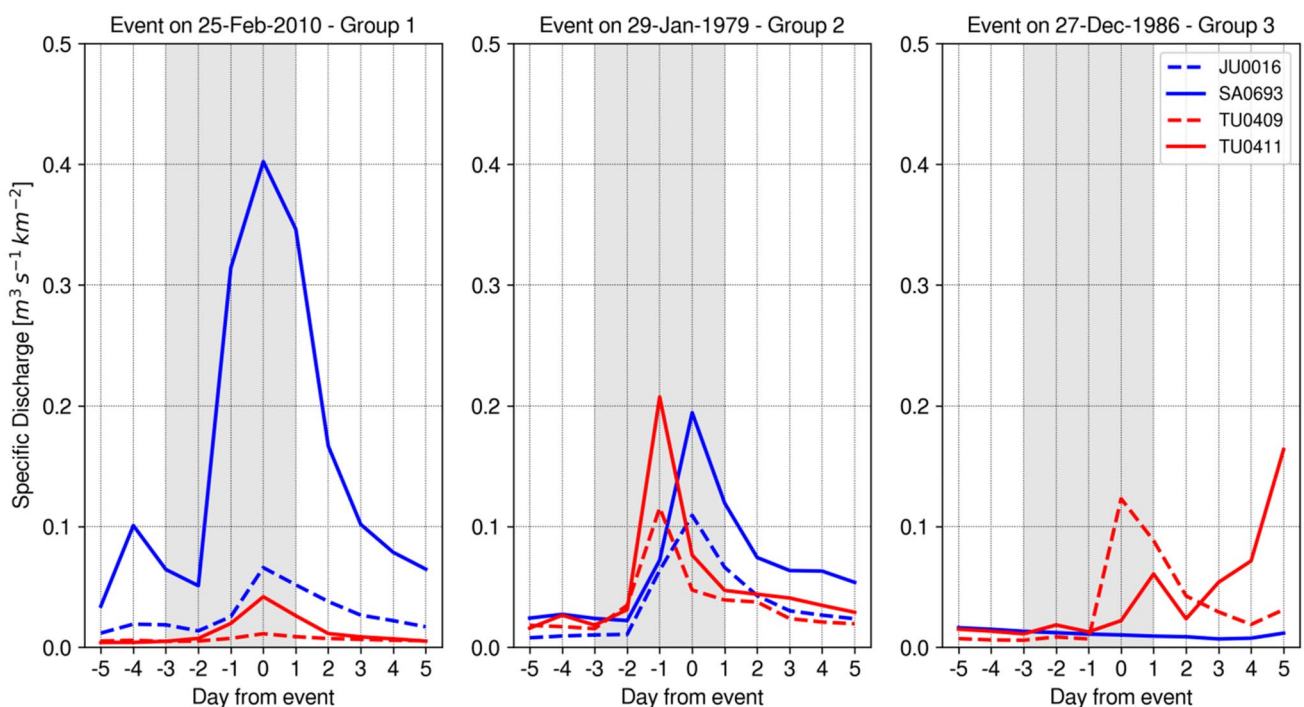


**Fig. 4** Daily specific-discharge observations of 11-days long sequences centered on the day of the reference events on 25th February, 2010, 29th Jan 1979, and 27th Dec 1986. For each event, the observation from the gauge stations of the Upper Rio Bermejo (blue) and the Rio Dulce (red) are shown; for the Group 3, the observation of only one gauge station were available. (Left) Group 1: largely

affecting the Upper Rio Bermejo area, with particularly high peak-discharge values, but also producing moderate discharges in the downstream Rio Dulce area (TU0411). (Center) Group 2: high peak-discharge values both in the Rio Bermejo and in the Rio Dulce, especially in the downstream regions. (Right) Group 3: affecting the Rio Dulce basin, particularly in the semi-arid area (TU0409)

Fig. 4, central panel). This event exhibits a few similar atmospheric dynamical features as the event representative of Group 1 (February, 25th, 2010) but also shows some important differences: The similarities are the development and intensification of a southerly flux of colder and drier than normal air masses to the east of the Central Andes, reaching a maximum anomaly of specific-humidity advection by Day - 1 for the study area (Fig. 6, central panels). Also, the north-westerly wind anomaly

before the event day in the east of the Central Andes was much weaker and confined to latitudes lower than 20° S, compared with what typically occurs for events of Group 1. Furthermore, we observe that the negative air-temperature anomaly established by Day - 1 was initially confined to the low-levels but extended up to the upper troposphere by Day 1 and eastwards to SESA (Fig. 6, right panels).

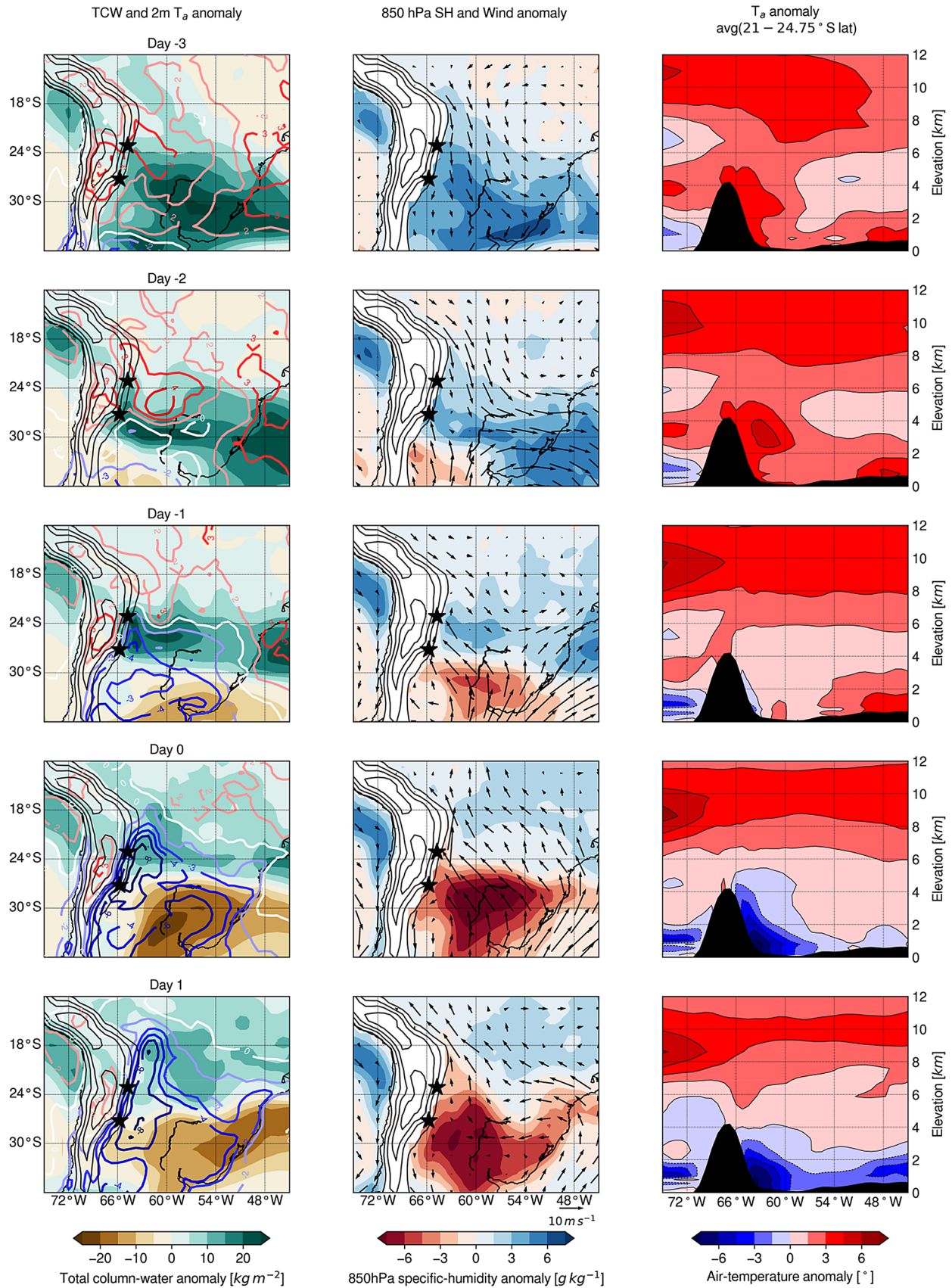


**Fig. 5** ERA-Interim surface and three-dimensional data for the extreme discharge event that occurred on February, 25th, 2010, representative of Group 1. Anomalies for 5-day time-lagged sequences (3 days before, event day, one day after) are shown for: (left) total water column (TWC, shades) and 2 m air temperature (red and blue isolines indicate positive and negative anomalies, respectively); (center) 850 hPa specific humidity (SH, shades) and wind speed and direction (arrows) anomalies. Values of the 850 hPa surface resulting below the Andean topography are masked; (right) air-temperature longitudinal cross-section ( $T_a$ , average between 21° and 24.75° S, shades) from the surface up to the high troposphere; the filled black polygon indicates the average topography between 21° and 24.75° S. Black stars show the center of the basins of the Upper Rio Bermejo and the Rio Dulce

Group 3 (7 events): The representative event occurred on December, 27th, 1986, and affected the Rio Dulce river basin, resulting in particularly large discharge volumes in the upper and semi-arid area of the catchment with peak-discharge values almost 30-times larger than the average annual discharge (Table S3, Supplementary material, and Fig. 4, right panel). The atmospheric features and evolution associated with this event were different compared to the other representative events described above: We observe an intense north-westerly wind anomaly to the east of the Central Andes confined to latitudes as low as 18° S and extended to the east coast of the continent (Fig. 7, central panels). A positive air-temperature anomaly at every level was present in the proximity of the eastern flank of the mountain range. In contrast to the event patterns in Group 1 and 2, this warm anomaly at the mountain front was associated with a deep colder and drier than normal cyclonic structure present at every level centered over the southern Brazilian coastal area, extending towards north-west (Fig. 7, central and right panels). By Day -2 the north-westerly wind anomaly intensified, reaching its maximum by Day -1, with high moisture advection at low-levels in association with a south/south-easterly wind flow to the east of the southern Central Andes. This south-easterly flow anomaly was controlled by a colder and drier cyclonic core located in South Brazil, resulting in a partial attenuation of the warm anomaly located at the eastern flank of the southern Central Andes (Fig. 7, central and right panels).

## 5 Discussion

### 5.1 Discharge-events analysis

In the southern Central Andes the steep topographic and environmental gradients with varying hillslope angles, soil types and thicknesses, and vegetation conditions (Bookhagen and Strecker 2012; Olen and Bookhagen 2020) will either dampen or amplify large rainfall events and impact the frequency distribution of river discharge. Due to different sources of nonlinearity in the transformation

of rainfall to runoff, daily precipitation distributions are often much lighter tailed than those of river discharge (Turcotte and Greene 1993; Malamud and Turcotte 2006). The shape of the frequency distribution of daily observations is commonly used to describe hydro-meteorological variability, with high variability associated with heavy-tailed distributions (Turcotte and Greene 1993; Malamud and Turcotte 2006; Molnar et al. 2006). Although our dataset is limited in number, we observed that specific-discharge variability is more pronounced in the predominantly semi-arid (heavier tail) than in the predominantly humid areas (lighter tail, Fig. 2 a). The difference lies in the ratio of number of smaller discharge magnitudes of intermediate events ( $Q_{0.2 \text{ year}}$ ) to larger magnitude of rare events ( $Q_{20 \text{ years}}$ ): the semi-arid environment of the Rio Dulce shows a smaller number of intermediate events than the humid Upper Rio Bermejo. Based on the analysis of the frequency distributions of runoff and rainfall, Rossi et al. (2016) have shown a similar behavior in the contiguous U.S. and Puerto Rico, i.e., increased runoff variability in arid environments is linked to reductions in the magnitude of intermediate events and not necessarily to an increase in the magnitude of rare events. This outcome has crucial implications not only for the relationship between storm depth and rare floods (> 99.9th percentile), which is characterized by pronounced nonlinearity in the transformation of rainfall to river discharge, but also on the efficiency of the erosional regime that controls the geomorphic processes shaping the landscape (Bookhagen and Strecker 2012; Castino et al. 2016). Because rare-event magnitudes present relatively small differences between predominantly semi-arid and humid catchments, significantly smaller intermediate-event magnitudes in the semi-arid catchments will result being less erosive than in the humid areas (Rossi et al. 2016).

We also observed that the distributions of the available rainfall time series from different gauge stations vary over narrow ranges of both intermediate and rare events and present similar shape and scale parameters independent of the type of the climatic environment (Fig. 2b). This observation suggests that the rainfall observations available in this area are representative of local-scale precipitation processes and cannot capture the overall hydro-climatic condition of the catchment where they are located. A previous study has analyzed the changes of discharge frequency distributions between 1940 and 1999 and it has been observed that the high spatiotemporal stochasticity and intermittency of rainfall-related processes and the sparse and disparately distributed rainfall stations will strongly limit the ability of the local rainfall network to fully capture the spatiotemporal scale of convective storms (Castino et al. 2016). Therefore, in a region with pronounced climatic gradients, such as the eastern Central Andes, river discharge can provide a better measure of hydro-meteorological variability than rainfall,

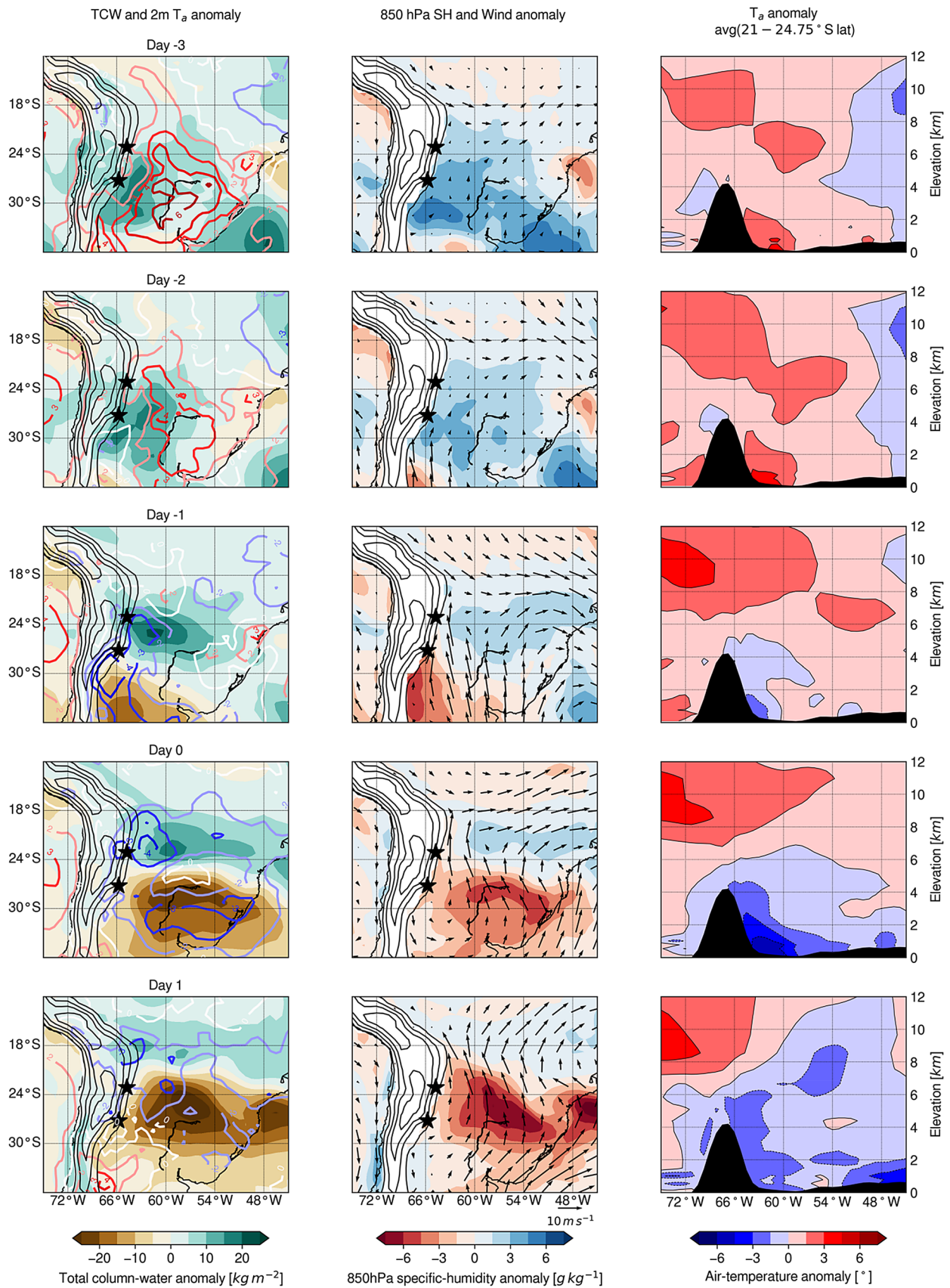


**Fig. 6** As in Fig. 5 but for the extreme discharge event occurred on January, 29th, 1979, representative of Group 2

integrating the storms' distribution and the response of the landscape at the catchment scale. This observation confirms the need of identifying extreme hydro-meteorological events in the study area using discharge observations from gauge stations draining either upper or lower portions of both the Upper Rio Bermejo and the Rio Dulce catchments.

## 5.2 Causes of extreme discharge events at the eastern flank of the southern Central Andes

The time-lagged climatological composites of geopotential height and wind (Fig. 3) document the importance in extreme-rainfall generation represented by the incursion of mid-latitude waves to the east of the Andes Mountain into subtropical and tropical latitudes. This cold surge is a previously documented process that largely affects the South American climate with a periodicity of 1–2 weeks and has its largest impact on precipitation during the wet season (Marengo et al. 1997; Garreaud and Wallace 1998; Garreaud 2000; Lupo et al. 2001; Vera and Vigliarolo 2002; Boers et al. 2015; Hurley et al. 2015; Rasmussen and Houze 2016). A particularly important atmospheric feature of cold surges is the deepening of the low-pressure system to the east of the Central Andes before the event (approximately 2–3 days). This low-pressure cell is accompanied by the intensification of the low-level meridional wind which becomes particularly strong prior the event day, as it is shown in the climatological composites (Fig. 3, left panels, from Days – 3 to Days – 1). The strength of this low-pressure system is also confirmed by the large statistical significance of the composites of the geopotential-height anomaly (Fig. S6, Supplementary material). The intensification of the low-level meridional wind has been recognized as the strengthening of the SALLJ, resulting in a higher than normal advection of warm and moist air masses from the Amazon basin (Garreaud 2000; Rasmussen and Houze 2016).

The above described features are also present in the composites restricted to extreme discharge events of Group 1 (Fig. 8; 5% significance of the anomalies are shown in Fig. S7, Supplementary material). Less consistency with the key features of cold-surge events was found with events of Group 2 and almost none with Group 3 (Figs. S8–11, Supplementary material). We hypothesize that Group 1 is controlled by cold-surge events, representing the largest group of events obtained from our classification (39%), and thus overprints the climatological composites of all events. In the following paragraphs, we will separately discuss the three events groups' phenomenology, extending our analysis to the mesoscale features associated with the representative events of each group.

For Group 1, by Day – 1 a fast-moving frontal zone developed between the anomalously warm and moist air

transported to the east of the Central Andes by an intensified SALLJ and the cool air advected by the meridional pressure gradient due to the transition of the ridge of the mid-latitude wave over the Andes (Fig. 5, central panels). This frontal zone was characterized by strong low-level convergence that provided sustained forcing for the development of intense mesoscale convective storms. It has been observed that summertime cold surges are accompanied by deep convection at the leading edge of the cool air moving equatorward from the southern subtropics associated with the strong low-level convergence embedded in a conditionally unstable environment (Garreaud 2000). This band of enhanced convection usually moves from the southern subtropics (about 35° S) into lower latitudes (~5° S) in about four days. Garreaud and Wallace (1998) estimated that convective precipitation associated with cold-surge events account on average for about 50% of the total summertime precipitation south of 25° S. In addition, in a study on the influence of topography on the initiation of convective systems in sub-tropical South America, Rasmussen and Houze (2016) evidenced that intensified low-level low pressure and SALLJ associated with a synoptic mid-latitude wave encountering the Andes are key elements for the development of severe storms with extreme horizontal dimension in the La Plata Basin. Therefore, given the above described features of their atmospheric dynamics, most of the extreme discharge events of Group 1 might be ascribed to the well-known cold-surge events, associated with deep convective storms resulting in large river discharges, particularly strong in the Upper Rio Bermejo (Fig. 4, left panel).

The visual inspection of the surface and three-dimensional 5-day time-lagged sequences of the ERA-Interim data of each event in Group 1 shows that 11 out of 15 events were triggered by cold surges. In addition, 2/3 of these events were recorded by the gauge stations draining the more humid portion of the study area and the remaining 1/3 by those relevant to semi-arid portion. This observation suggests that extremely intense convective storms developing to the east of the southern Central Andes in association with cold surges tend to affect twice as often the downstream as the upstream portion of this region. The remaining events of Group 1 (i.e., not associated with enhanced SALLJ and the migration of a cold front as in the case of cold surges), revealed anomalously warm and moist low-level air transported from the tropics to the east of the Central Andes prior the event day. Subsequently, the strong southerly wind anomaly likely forced the advection of these moist air masses against the steep topography of the study area, thus resulting in intense orographic rainfall (Houze 2012; Espinoza et al. 2015). We suggest that the limited heterogeneity of the atmospheric circulation is a potential explanation for the weaker negative anomaly of 2 m air temperature obtained on day 0 and day + 1 for the composite of Group 1 compared with its

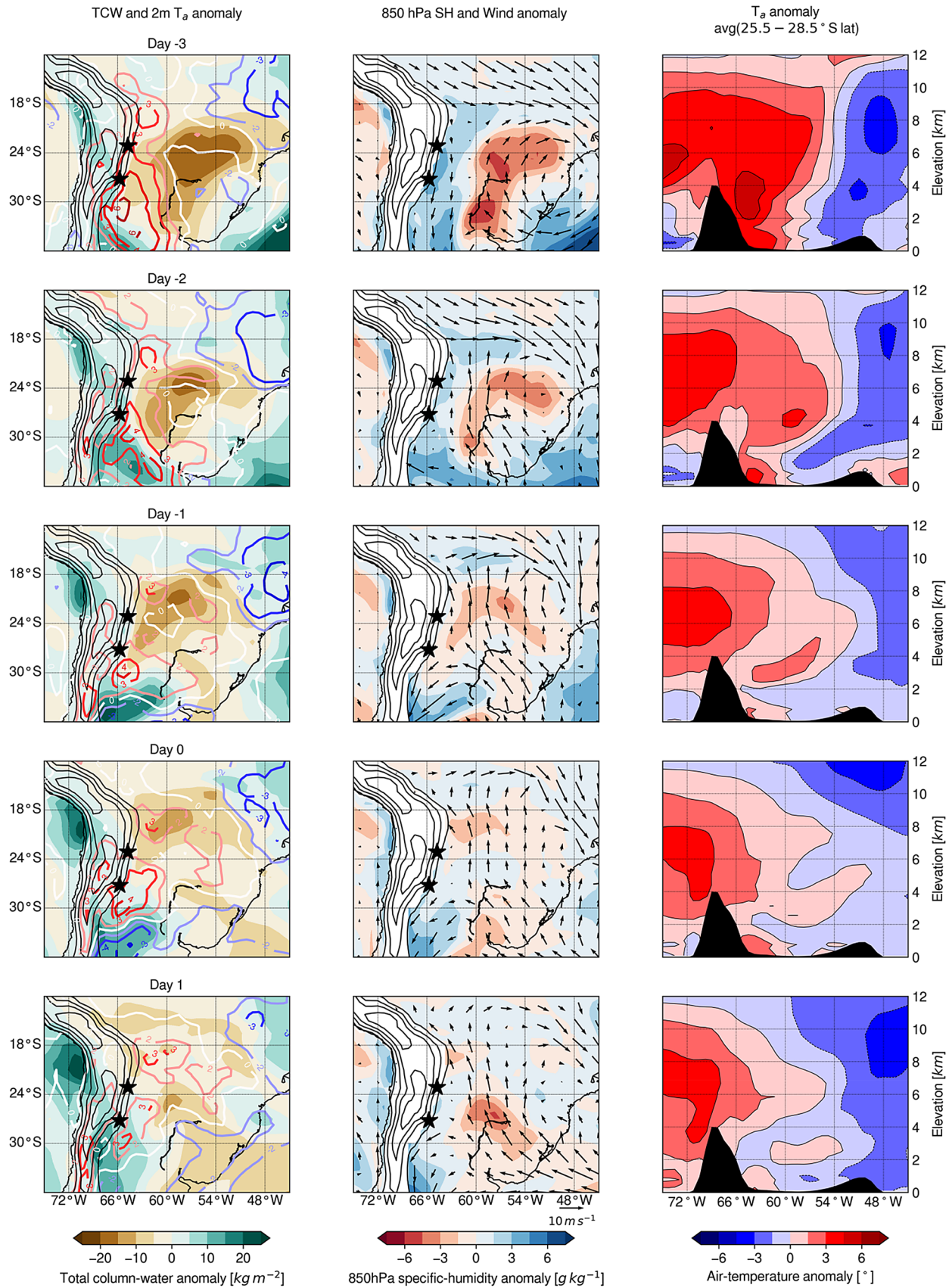


**Fig. 7** As in Fig. 5 but for the extreme discharge event occurred on December, 27th, 1986, representative of Group 3. The air-temperature longitudinal cross-section and the average topography (filled black polygons) are obtained averaging between 25.5° and 28.5° S

representative extreme event (Figs. 5, 8). We investigated the possible causes for this discrepancy, by identifying for each event the geographical location and magnitude of the minimum of the 2 m air-temperature anomaly by each day of the 5-days sequences (Fig. S12, Supplementary material). Although by day 0 and day + 1 the minimum magnitude of the 2 m air-temperature anomaly is below  $-2\text{ }^{\circ}\text{C}$  for most of the events, this analysis shows that these minimum values are rather sparsely distributed for all days, confirming our hypothesis that the composites produced statistically non-significant mean values for the 2 m air-temperature anomaly because of the relative spatial heterogeneity of this field between the events within Group 1.

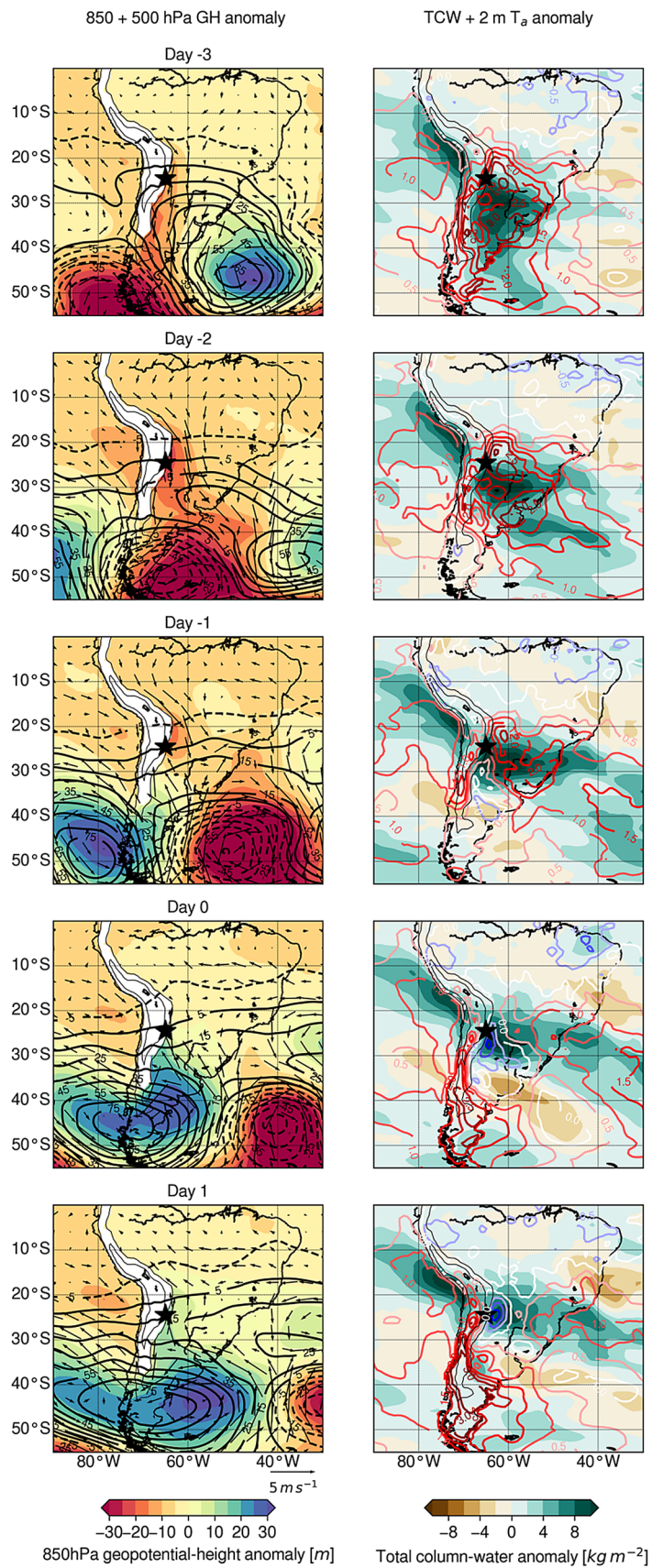
For Group 2, the climatological composite maps show that these events present large dynamical similarities with cold surges, e.g. the westerly migration of an upper-level mid-latitude wave, also visible at the middle troposphere, resulting in an incursion of cooler and drier than normal air from the high latitudes towards the subtropics starting by Day  $-2$  (Fig. 6). In this case, we observe a frontal zone, extending in north-east direction between the anomalously warm and wet air to the east of the Andes and the southerly cooler air, accompanied by strong low-level southerly winds. However, the climatological composite maps show the deepening of the low-level low-pressure cell and the intensified SALLJ to the east of the Andes mostly at latitudes equatorward of  $20^{\circ}\text{ S}$ . In addition, from the representative event of Group 2 we observe that the warm and moist air prior to the event was not confined just to the immediate area to the east of the Central Andes as for the event of Group 1 (Fig. 5, right panel, Days  $-3$  and  $-2$ ), but largely extended to the SESA region (Fig. 6, left panels, Days  $-3$  and  $-2$ ). Also, the cold air incursion was not limited to the low- and middle-levels, but reached the upper levels of the troposphere (Figs. 5, 6, right panels, Days 0 and 1). Nevertheless, we envision that, in an anomalously warm and moist atmospheric environment, the strong low-level convergence at the leading edge of the cold incursion might have triggered the formation of mesoscale convective storms to the east of the southern Central Andes. Such strong rainstorms resulted in intense precipitation which diffusively affected the study region, although with relatively lower peak values compared to the representative event of Group 1 (Fig. 4, central and left panels). Furthermore, we suggest that the above described discrepancies might depend on the position and intensity of the Bolivian High or the extension and strength of the mid-latitude pressure dipole that can

result in a slower migration of the high-pressure cell or a blocking activity of the low-pressure cell over the southwestern Atlantic Ocean (Fig. S8, Supplementary material). Importantly, the visual inspection of each event relevant to Group 2 showed that almost all of them (10 out of 11) were triggered by atmospheric conditions similar to cold surges and, by virtue of these key similarities, we coined these events ‘modified cold surge’. In contrast with Group 1, 2/3 of these events were recorded by the gauge stations draining the upstream basin portions and the remaining 1/3 were recorded in the downstream regions of the study area. This observation suggests that extremely intense convective storms developing to the east of the southern Central Andes in association with ‘modified cold surges’, tend to affect twice as often the high-elevation areas than the lower and more humid portion of this region.

For Group 3 (Fig. 7), the climatological composite maps of these events revealed a different atmospheric pattern from those previously identified in Group 1 and 2. The atmospheric circulation was initially dominated at large scale by an anomalously intense and extensive high-pressure cell over the west South Atlantic Ocean associated with a large positive air-temperature anomaly at low levels in southern South America (Day  $-3$ , Fig. S10, Supplementary material). This pressure system gradually weakened under the effect of the migration of a mid-latitude trough from the east South Pacific, which in turn deepened as it crossed the Andean mountain and reached the west South Atlantic (Day  $-1$  and Day 0). At the same time, this low-pressure cell was quickly followed by a high-pressure cell (from Day  $-1$  to Day + 1) advecting cooler air masses from high latitudes to the subtropics, similarly to the cold-surge events (Fig. S10, Supplementary material). From the meso- to the synoptic-scale, we observed the presence of a frontal structure at low levels to the east of the southern Central Andes (Fig. 7, Day  $-3$ ). This front developed between the northerly moist and warm flux from the tropics alongside the Andean mountains and the southeasterly cooler air masses advected by a cyclone already at its mature stage and located at the coast of southern Brazil (Fig. 7, Day  $-3$ ). Likely, the strong low-level convergence associated with this frontal structure triggered the development of rainfall in a mesoscale convective system that resulted in high river discharges in the Rio Dulce river basin (Fig. 4, right panel). Generally, we observe a higher heterogeneity of the atmospheric dynamics at meso- and synoptic-scale in Group 3 in comparison to the other two groups. This is further confirmed by the low significance of the anomaly values of its composite (Figs. S7, S9, S11, Supplementary material).

Overall, our analysis identified 21 out of 40 (53%) extreme discharge events to be associated with cold surges or with atmospheric processes similar to cold surges. It emerges that these climatic features result in extreme discharges in

**Fig. 8** As in Fig. 3 but for the climatological composite of ERA-Interim data relevant to extreme discharge events of Group 1





both drainage basins with similar frequency of occurrence. We emphasize that our analysis does not represent a quantitative estimation of the contribution of cold surges to annual discharge totals, because we only analyzed the conditions of extreme hydro-meteorological events (> 99.9th percentile). Nevertheless, it documents the importance of cold surges for discharge anomalies in the eastern flank of the southern Central Andes.

Our observation is in good agreement with other studies. According to a sea-level pressure-pattern classification over southern South America, the ‘cold-surge mode’ results as the second-most recurrent synoptic pattern after zonal circulation (Compagnucci and Salles 2002) and cold-surge events account on average for about 50% of the total summertime precipitation south of 25° S (Garreaud and Wallace 1998; Garreaud 2000). In addition, it has been observed that during the development of cold surges the associated transient mid-latitude waves undergo strong amplification and their amplitude is given by the superposition of fast-moving, synoptic-scale waves and quasi-stationary, planetary waves (Krishnamurti et al. 1999; Garreaud 2000). In a recent study, Boers et al. (2019) have suggested that upper-level Rossby waves likely control a global rainfall-teleconnection pattern which is responsible for long-distance (> 2500 km) coupling of extreme rainfall events. These authors showed that extreme-rainfall events in the monsoon systems of south-central Asia, East Asia, and Africa are synchronized and revealed concise links between south-central Asia and the European and North American extra-tropics, as well as the Southern-Hemisphere extra-tropics.

## 6 Conclusions

Past studies highlight the high dynamics and varying trends of rainfall patterns in South America and there are several causes for hydro-meteorological extreme events. In the southern Central Andes, we identified propagating cold fronts as one important trigger mechanisms for the strongest hydrologic events.

We analyzed the atmospheric dynamics at large- and meso-scales associated with extreme discharge events (> 99.9th percentile) representing the strongest 40 distinct events in the southern Central Andes from 1979 to 2016. We rely on daily rainfall ( $n = 11$ ) and river-discharge ( $n = 9$ ) gauge time series starting from 1940 in tributaries of the Upper Rio Bermejo and the Rio Dulce in NW Argentina. We performed a detailed analysis of their magnitude-frequency distributions for these semi-arid and humid areas. The associated atmospheric conditions of the identified extreme events were investigated with reanalysis data. Our study suggests that to the east of the southern Central Andes (20°–30°S) one of the most important climatic features

controlling the formation of intense mesoscale convective systems is caused by low- to middle-level temperature changes associated with cold surges. These are often linked with the passage of mid-latitude waves over South America during the monsoon season. We make the following three key observations:

1. For the period between 1940 and 2016, daily rainfall observations from the semi-arid and humid areas do not show significant differences in their magnitude-frequency relations. On the contrary, the distributions of daily specific discharge exhibit more pronounced variability with a heavier tail for the southern semi-arid Rio Dulce river basin than for the northern Upper Rio Bermejo river basin with more humid conditions. Importantly, in the semi-arid environment this difference is characterized by fewer discharge events with intermediate magnitude (0.2 year mean return period, i.e. > 98th percentile) than in the humid environments, whereas the number of rare events (20 years mean return period, i.e. > 99.9th percentile) is comparable in the two areas. The rainfall distributions for the two catchments do not exhibit a similar behavior, evidencing the strong nonlinear relationship between rainfall and discharge, especially in case of storm events and rare floods. Based on our analysis, we argue that discharge data are more suitable than rainfall observations for identifying extreme hydro-meteorological events and their impact on geomorphologic processes.
2. The climatological composites of the 5-day time-lagged sequences of geopotential height in the middle (500 hPa) and upper (200 hPa) troposphere for the selected 40 extreme discharge events showed a weak mid-latitude transient pressure dipole that crosses southern South America. The high-pressure core of this dipole moves eastward from the Pacific Ocean and crosses the Andes at the day before the event, forcing the advection of dry and cold air masses from higher latitudes into the continent. As a result, a cold front is established at low levels between these air masses advected from high latitudes and a low-pressure system to the east of the Central Andes associated with warmer and more humid than normal air masses. These atmospheric features are typical of cold surges, i.e., the incursion of mid-latitude waves to the east of the Andes into sub-tropical and tropical latitudes which strongly affect the South-American precipitation pattern in particular during the wet season.
3. By applying a subjective classification scheme, we obtained three groups of extreme discharge events representing 80% of all events. For each group we generated the climatological composites and described representative atmospheric processes and dynamics for a case-study event. These analyses showed that in the

study area extreme discharge events are mainly associated with the north-northeastward migration of frontal systems. For 53% of all the extreme discharge events, this frontal zone is a cold front, characterized by strong low-level convergence which provides sustained forcing for intense mesoscale convective systems, a key feature of cold surges. The remaining extreme events can be described as highly heterogeneous atmospheric patterns, such as strong cyclonic activity in south-eastern Brazil or events of the South American Low-Level Jet occasionally associated with frontal systems developing at the edge of low-level south-southeasterly warm air flows.

**Acknowledgements** We thank the Deutsche Forschungsgemeinschaft (DFG) and the Brandenburg Ministry of Science, Research and Cultural Affairs, Germany, within the framework of the international research training group IGK2018 SuRfAce processes, Tectonics and Georesources: The Andean foreland basin of Argentina (StRATEGY) and NEXUS: Earth Surface Dynamics for financial support. The authors thank the Subsecretaría de Recursos Hídricos (BDHI) and the Servicio Meteorológico Nacional, Argentina, for providing rainfall and river-discharge time series, and the European Centre for Medium-Range Weather Forecasts (ECMWF), for providing the ERA-Interim reanalysis data. The authors thank two anonymous reviewers for their comments and are also thankful to Roberto Bignone and Matteo Corazza for the interesting discussions about the hydrological measurements and the reanalysis data.

**Funding** Open Access funding enabled and organized by Projekt DEAL.

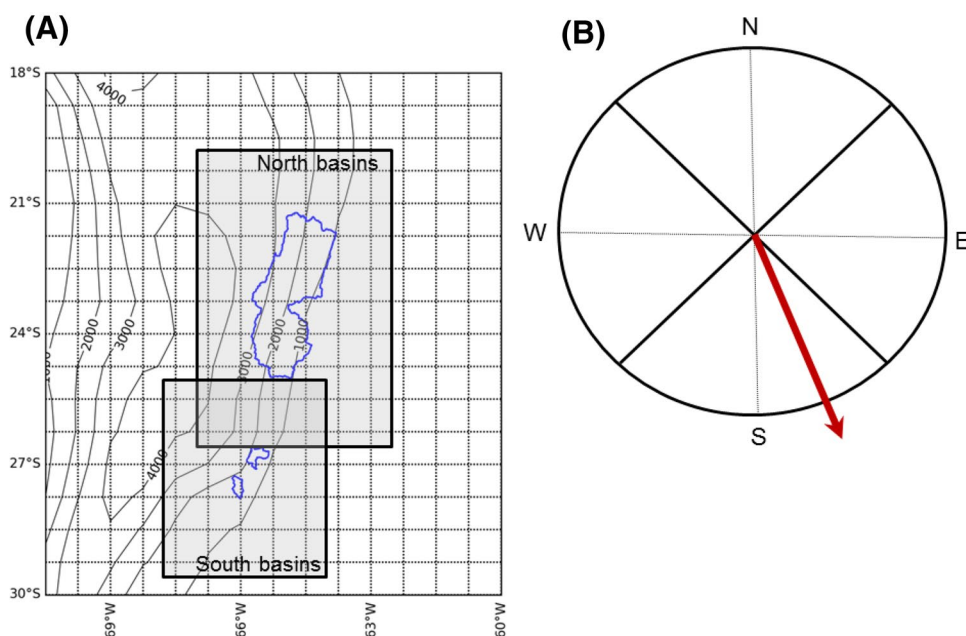
**Open Access** This article is licensed under a Creative Commons Attribution 4.0 International License, which permits use, sharing, adaptation, distribution and reproduction in any medium or format, as long as you give appropriate credit to the original author(s) and the source,

provide a link to the Creative Commons licence, and indicate if changes were made. The images or other third party material in this article are included in the article's Creative Commons licence, unless indicated otherwise in a credit line to the material. If material is not included in the article's Creative Commons licence and your intended use is not permitted by statutory regulation or exceeds the permitted use, you will need to obtain permission directly from the copyright holder. To view a copy of this licence, visit <http://creativecommons.org/licenses/by/4.0/>.

## Appendix: Subjective classification of discharge events using the prevailing direction of moisture-flux anomaly sequences

The aim of the analysis is to decipher whether the wind of the Upper Rio Bermejo and Rio Dulce basins (Fig. 9a) is zonal (westerly or easterly) or meridional (northerly or southerly) during the 5-day time-lagged sequences of the extreme discharge events. Therefore, four 90° wide directional sectors are considered, centered on the cardinal directions and associated with zonal and meridional fluxes (Fig. 9b). For deciphering the evolution of the wind direction of each 5-day time-lagged sequence, the following method is applied: First, the area where the gauge station associated with the discharge event is identified (North or South basins, Fig. 9a); second, the frequency distribution of the direction of the wind anomaly is estimated according to the four directional sectors using the values at the masked grid points of the identified area (North or South basins). The daily prevailing direction is given by the directional sector that has the maximum frequency and its frequency is at least equal to the 50th

**Fig. 9** **a** The two areas for deciphering the prevailing wind direction: (1) North basins, for the Upper Rio Bermejo [62.25–66 W/20.25–26.25 S], including 34 masked grid nodes; (2) South basins, for the Rio Dulce [63.75–66.75 W/25.5–29.25 S], with 23 masked grid nodes. **b** The four 90° wide directional sectors: meridional-southerly [45°, 135°], zonal-easterly [135°, 225°], meridional-northerly [225°, 315°], zonal-westerly [–45°, 45°]. As example, the red arrow indicates a meridional-northerly wind



percentile; if both conditions are not satisfied, the prevailing wind direction is considered as undefined. As example, the red arrow indicates a meridional-northerly wind (Fig. 9(B)).

## References

- Antolini G, Auteri L, Pavan V et al (2015) A daily high-resolution gridded climatic data set for Emilia-Romagna, Italy, during 1961–2010. *Int J Climatol*. <https://doi.org/10.1002/joc.4473>
- Barichivich J, Gloor E, Peylin P et al (2018) Recent intensification of Amazon flooding extremes driven by strengthened Walker circulation. *Sci Adv* 4:ea8785. <https://doi.org/10.1126/sciadv.aat8785>
- Bianchi AR, Yañez CE (1992) Las precipitaciones en el Noroeste Argentino. *Inst. Nac. Tecnol. Agropecu. Estación Exp*
- Boers N, Rheinwalt A, Bookhagen B et al (2014) The South American rainfall dipole: a complex network analysis of extreme events. *Geophys Res Lett* 41:7397–7405. <https://doi.org/10.1002/2014GL061829>
- Boers N, Bookhagen B, Marwan N, Kurths J (2015) Spatiotemporal characteristics and synchronization of extreme rainfall in South America with focus on the Andes Mountain range. *Climate Dyn*. <https://doi.org/10.1007/s00382-015-2601-6>
- Boers N, Goswami B, Rheinwalt A et al (2019) Complex networks reveal global pattern of extreme-rainfall teleconnections. *Nature*. <https://doi.org/10.1038/s41586-018-0872-x>
- Boilley A, Wald L (2015) Comparison between meteorological re-analyses from ERA-Interim and MERRA and measurements of daily solar irradiation at surface. *Renew Energy* 75:135–143. <https://doi.org/10.1016/j.renene.2014.09.042>
- Bookhagen B (2016) Glaciers and monsoon systems. In: de Carvalho LMV, Jones C (eds) *The monsoons and climate change: observations and modeling*. Springer International Publishing, Cham, pp 225–249
- Bookhagen B, Burbank DW (2010) Toward a complete Himalayan hydrological budget: Spatiotemporal distribution of snowmelt and rainfall and their impact on river discharge. *J Geophys Res* 115:F03019. <https://doi.org/10.1029/2009JF001426>
- Bookhagen B, Strecker MR (2008) Orographic barriers, high-resolution TRMM rainfall, and relief variations along the eastern Andes. *Geophys Res Lett* 35:L06403. <https://doi.org/10.1029/2007GL032011>
- Bookhagen B, Strecker MR (2012) Spatiotemporal trends in erosion rates across a pronounced rainfall gradient: examples from the southern Central Andes. *Earth Planet Sci Lett* 327–328:97–110. <https://doi.org/10.1016/j.epsl.2012.02.005>
- Compsetella CM, Vera CS (2002) The influence of the Andes mountains on the South American low-level flow. *Geophys Res Lett* 29:1826. <https://doi.org/10.1029/2002GL015451>
- Carvalho LMV, Jones C, Liebmann B (2002) Extreme precipitation events in Southeastern South America and large-scale convective patterns in the South Atlantic convergence zone. *J Clim* 15:2377–2394
- Carvalho LMV, Jones C, Liebmann B (2004) The South Atlantic convergence zone: intensity, form, persistence, and relationships with intraseasonal to interannual activity and extreme rainfall. *J Climate* 17:88–108
- Carvalho LMV, Jones C, Posadas AND et al (2012) Precipitation characteristics of the South American monsoon system derived from multiple datasets. *J Climate* 25:4600–4620. <https://doi.org/10.1175/JCLI-D-11-00335.1>
- Castino F, Bookhagen B, Strecker MR (2016) River-discharge dynamics in the Southern Central Andes and the 1976–77 global climate shift. *Geophys Res Lett* 43:11679–11687. <https://doi.org/10.1002/2016GL070868>
- Castino F, Bookhagen B, Strecker MR (2017a) Rainfall variability and trends of the past six decades (1950–2014) in the subtropical NW Argentine Andes. *Climate Dyn* 48:1049–1067. <https://doi.org/10.1007/s00382-016-3127-2>
- Castino F, Bookhagen B, Strecker MR (2017b) Oscillations and trends of river discharge in the southern Central Andes and linkages with climate variability. *J Hydrol*. <https://doi.org/10.1016/j.jhydrol.2017.10.001>
- Cohen JCP, Silva Dias MAF, Nobre CA (1995) Environmental conditions associated with Amazonian squall lines: a case study. *Mon Weather Rev* 123:3163–3174
- Compagnucci RH, Salles MA (2002) Surface pressure patterns during the year over Southern South America. *Int J Climatol* 17:635–653. [https://doi.org/10.1002/\(sici\)1097-0088\(199705\)17:6<635:aid-joc81>3.3.co;2-2](https://doi.org/10.1002/(sici)1097-0088(199705)17:6<635:aid-joc81>3.3.co;2-2)
- Compagnucci RH, Araneo D, Canziani PO (2001) Principal sequence pattern analysis: a new approach to classifying the evolution of atmospheric systems. *Int J Climatol* 21:197–217. <https://doi.org/10.1002/joc.601>
- da Silva A, de Carvalho L (2007) Large-scale index for South America Monsoon (LISAM). *Atmos Sci Lett*. <https://doi.org/10.1002/asl>
- de la Torre A, Hierro R, Llamedo P et al (2011) Severe hailstorms near Southern Andes in the presence of mountain waves. *Atmos Res* 101:112–123. <https://doi.org/10.1016/j.atmosres.2011.01.015>
- Dee DP, Uppala SM, Simmons AJ et al (2011) The ERA-Interim reanalysis: configuration and performance of the data assimilation system. *Q J R Meteorol Soc* 137:553–597. <https://doi.org/10.1002/qj.828>
- Di Baldassarre G, Montanari A (2009) Hydrology and earth system sciences uncertainty in river discharge observations: a quantitative analysis. *Hydrol Earth Syst Sci* 13:913–921
- Dralle DN, Karst NJ, Charalampous K et al (2017) Event-scale power law recession analysis: quantifying methodological uncertainty. *Hydrol Earth Syst Sci* 21:65–81. <https://doi.org/10.5194/hess-21-65-2017>
- Durkee JD, Mote TL, Shepherd JM (2009) The contribution of mesoscale convective complexes to rainfall across subtropical South America. *J Climate* 22:4590–4605. <https://doi.org/10.1175/2009JCLI2858.1>
- Enfield DB, Mestas-Nunez AM (1999) How ubiquitous is the dipole relationship in tropical Atlantic sea surface temperatures? *J Geophys Res* 40:7841–7884
- Espinoza JC, Lengaigne M, Ronchail J et al (2012) Large-scale circulation patterns and related rainfall in the Amazon Basin: a neuronal networks approach. *Climate Dyn* 38:121–140. <https://doi.org/10.1007/s00382-011-1010-8>
- Espinoza JC, Chavez S, Ronchail J et al (2015) Rainfall hotspots over the southern tropical Andes: spatial distribution, rainfall intensity, and relations with large-scale atmospheric circulation. *Water Resour Res* 6:446. <https://doi.org/10.1002/2014WR016273>
- Espinoza JC, Ronchail J, Marengo J et al (2019) Contrasting North-South changes in Amazon wet-day and dry-day frequency and related atmospheric features (1981–2017). *Climate Dyn*. <https://doi.org/10.1007/s00382-018-4462-2>
- Gabet E, Burbank D, Prattsitaula B et al (2008) Modern erosion rates in the High Himalayas of Nepal. *Earth Planet Sci Lett* 267:482–494. <https://doi.org/10.1016/j.epsl.2007.11.059>
- Gandu AW, Geisler JE (1991) A primitive equations model study of the effect of topography on the summer circulation over tropical South America. *J Atmos Sci* 48:1822–1836. [https://doi.org/10.1175/1520-0469\(1991\)048<1822:APEMSO>2.0.CO;2](https://doi.org/10.1175/1520-0469(1991)048<1822:APEMSO>2.0.CO;2)

- Gandu AW, Silva Dias PL (1998) Impact of tropical heat sources on the South American tropospheric upper circulation and subsidence. *J Geophys Res* 103:6001
- Garreaud RD (2000) Cold air incursions over subtropical South America: mean structure and dynamics. *Mon Weather Rev* 128:2544–2559
- Garreaud RD, Aceituno P (2001) Interannual rainfall variability over the South American Altiplano. *J Climate* 14:2779–2789
- Garreaud RD, Wallace JM (1998) Summertime incursion of mid-latitude air into subtropical and tropical South America. *Mon Weather Rev* 126:2713–2733. <https://doi.org/10.1242/dev.011759>
- Garreaud R, Vuille M, Clement AC (2003) The climate of the Altiplano: observed current conditions and mechanisms of past changes. *Palaeogeogr Palaeoclimatol Palaeoecol* 194:5–22. [https://doi.org/10.1016/S0031-0182\(03\)00269-4](https://doi.org/10.1016/S0031-0182(03)00269-4)
- Garreaud RD, Molina A, Farias M (2010) Andean uplift, ocean cooling and Atacama hyperaridity: a climate modeling perspective. *Earth Planet Sci Lett* 292:39–50. <https://doi.org/10.1016/j.epsl.2010.01.017>
- Gioannettone JP, Barros AP (2009) Probing regional orographic controls of precipitation and cloudiness in the Central Andes using satellite data. *J Hydrometeorol* 10:167–182. <https://doi.org/10.1175/2008JHM973.1>
- Halloy S (1982) Contribución al estudio de la zona de Huaca huasi, Cumbres Calchaquíes (Tucumán Argentina). Univ. Nac, Tucumán
- Hersch RW (1978) *Hydrometry principles and practices*. Wiley, Chichester
- Hodges KI, Lee RW, Bengtsson L (2011) A comparison of extratropical cyclones in recent reanalyses ERA-Interim, NASA MERRA, NCEP CFSR, and JRA-25. *J Climate* 24:4888–4906. <https://doi.org/10.1175/2011JCLI4097.1>
- Houze R (2012) Orographic effects on precipitating clouds. *Rev Geophys* 50:1–47. <https://doi.org/10.1029/2011RG000365.1> INTRODUCTION
- Huffman GJ, Bolvin DT, Nelkin EJ et al (2007) The TRMM multisatellite precipitation analysis (TMPA): quasi-global, multiyear, combined-sensor precipitation estimates at fine scales. *J Hydrometeorol* 8:38–55. <https://doi.org/10.1175/JHM560.1>
- Hurley JV, Vuille M, Hardy DR et al (2015) Cold air incursions,  $\delta^{18}\text{O}$  variability and monsoon dynamics associated with snow days at Quelccaya Ice Cap, Peru. *J Geophys Res* 120:7467–7487. <https://doi.org/10.1002/2015JD023323>
- Huth R, Beck C, Philipp A et al (2008) Classifications of atmospheric circulation patterns: recent advances and applications. *Ann N Y Acad Sci* 1146:105–152. <https://doi.org/10.1196/annals.1446.019>
- Krishnamurti TN, Tewari M, Chakraborty DR et al (1999) Downstream amplification: a possible precursor to major freeze events over Southeastern Brazil. *Weather Forecast* 14:242–270
- Lliboutry L (1998) *Glaciers of Chile and Argentina*. In: Williams RS, Ferrigno J (eds) *Glaciers of South America* USGS Professional Paper 1386-I. USGS, Denver, pp 109–206
- Lovino MA, Müller OV, Berbery EH et al (2018) How have daily climate extremes changed in the recent past over northeastern Argentina? *Glob Planet Change* 168:78–97. <https://doi.org/10.1016/j.gloplacha.2018.06.008>
- Luna LV, Bookhagen B, Niedermann S et al (2018) Glacial chronology and production rate cross-calibration of five cosmogenic nuclide and mineral systems from the southern Central Andean Plateau. *Earth Planet Sci Lett* 500:242–253. <https://doi.org/10.1016/j.epsl.2018.07.034>
- Lupo AR, Nocera JJ, Bosart LF et al (2001) South American cold surges: types, composites, and case studies. *Mon Weather Rev* 129:1021–1041. [https://doi.org/10.1175/1520-0493\(2001\)129<1021:sacstc>2.0.co;2](https://doi.org/10.1175/1520-0493(2001)129<1021:sacstc>2.0.co;2)
- Madden RA, Julian PR (1971) Detection of a 40–50 day oscillation in the zonal wind in the tropical Pacific. *J Atmos Sci* 28:702–708
- Maddox RA, Chappell CF, Hoxit LR (1979) Synoptic and mesoscale aspects of flash flood events. *Bull Am Meteorol Soc* 60:115–123
- Malamud BD, Turcotte DL (2006) The applicability of power-law frequency statistics to floods. *J Hydrol* 322:168–180. <https://doi.org/10.1016/j.jhydrol.2005.02.032>
- Mantua N, Hare S (2002) The Pacific decadal oscillation. *J Oceanogr* 58:35–44
- Marcato G, Pasuto A, Rivelli FR (2009) Mass movements in the Rio Grande Valley (Quebrada de Humahuaca, Northwestern Argentina): a methodological approach to reduce the risk. *Adv Geosci* 22:59–65
- Marcato G, Bossi G, Rivelli F, Borgatti L (2012) Debris flood hazard documentation and mitigation on the Tilcara alluvial fan (Quebrada de Humahuaca, Jujuy province, North-West Argentina). *Nat Hazards Earth Syst Sci* 12:1873–1882. <https://doi.org/10.5194/nhess-12-1873-2012>
- Marengo J, Cornejo A, Satyamurty P et al (1997) Cold surges in tropical and extratropical South America: the strong event in June 1994. *Mon Weather Rev* 125:2759–2786. [https://doi.org/10.1175/1520-0493\(1997\)125<2759:csitae>2.0.co;2](https://doi.org/10.1175/1520-0493(1997)125<2759:csitae>2.0.co;2)
- Marengo JA, Tomasella J, Uvo CR (1998) Trends in streamflow and rainfall in tropical South America: Amazonia, eastern Brazil, and northwestern Peru. *J Geophys Res* 103:1775. <https://doi.org/10.1029/97JD02551>
- Marengo JA, Soares WR, Saulo C, Nicolini M (2004) Climatology of the low-level jet east of the Andes as derived from the NCEP-NCAR reanalyses: characteristics and temporal variability. *J Climate* 17:2261–2280. [https://doi.org/10.1175/1520-0442\(2004\)017<2261:COTLJE>2.0.CO;2](https://doi.org/10.1175/1520-0442(2004)017<2261:COTLJE>2.0.CO;2)
- Marengo JA, Liebmann B, Grimm AM et al (2012) Recent developments on the South American monsoon system. *Int J Climatol* 32:1–21. <https://doi.org/10.1002/joc.2254>
- Molnar P, Anderson RS, Kier G, Rose J (2006) Relationships among probability distributions of stream discharges in floods, climate, bed load transport, and river incision. *J Geophys Res Earth Surf* 111:1–10. <https://doi.org/10.1029/2005JF000310>
- Mooney PA, Mulligan FJ, Fealy R (2011) Comparison of ERA-40, ERA-Interim and NCEP/NCAR reanalysis data with observed surface air temperatures over Ireland. *Int J Climatol* 557:545–557. <https://doi.org/10.1002/joc.2098>
- Mutzner R, Bertuzzo E, Tarolli P et al (2013) Geomorphic signatures on Brutsaert base flow recession analysis. *Water Resour Res* 49:5462–5472. <https://doi.org/10.1002/wrcr.20417>
- Olen S, Bookhagen B (2020) Application of SAR interferometric coherence time series: spatiotemporal dynamics of geographic transitions in the South-Central Andes. *JGR Earth Surf.* <https://doi.org/10.1029/2019JF005141>
- Paccini L, Espinoza JC, Ronchail J et al (2018) Intra-seasonal rainfall variability in the Amazon basin related to large-scale circulation patterns: a focus on western Amazon-Andes transition region. *Int J Climatol* 38:2386–2399. <https://doi.org/10.1002/joc.5341>
- Pasquini AI, Depetris PJ (2007) Discharge trends and flow dynamics of South American rivers draining the southern Atlantic seaboard: an overview. *J Hydrol* 333:385–399. <https://doi.org/10.1016/j.jhydrol.2006.09.005>
- Perry LB, Seimon A, Kelly GM (2014) Precipitation delivery in the tropical high Andes of southern Peru: new findings and paleoclimatic implications. *Int J Climatol* 34:197–215. <https://doi.org/10.1002/joc.3679>
- Plate EJ (2002) Flood risk and flood management. *J Hydrol* 267:2–11. [https://doi.org/10.1016/S0022-1694\(02\)00135-X](https://doi.org/10.1016/S0022-1694(02)00135-X)
- Poveda G, Jaramillo L, Vallejo LF (2014) Seasonal precipitation patterns along pathways of South American low-level jets and aerial rivers. *Water Resour Res* 50:98–118. <https://doi.org/10.1002/2013WR014087>

- Prince KC, Evans C (2018) A climatology of extreme South American Andean cold surges. *J Appl Meteorol Climatol*. <https://doi.org/10.1175/JAMC-D-18-0146.1>
- Rasmussen KL, Houze RA (2016) Convective initiation near the Andes in subtropical South America. *Mon Weather Rev* 144:2351–2374. <https://doi.org/10.1175/MWR-D-15-0058.1>
- Rodda JC (2011) Guide to hydrological practices. *Hydrol Sci J* 56:196–197
- Rohmeder W (1943) Observaciones meteorológicas en la región encumbrada de las Sierras de Famatina y del Aconquija (república Argentina). *An Soc Cient Arg* 136:97–124
- Romanschke U, Houze RA (2013) Characteristics of precipitating convective systems accounting for the summer rainfall of tropical and subtropical South America. *J Hydrometeorol*. <https://doi.org/10.1175/JHM-D-12-060.1>
- Rossi MW, Whipple KX, Vivoni ER (2016) Precipitation and evapotranspiration controls on daily runoff variability in the contiguous United States and Puerto Rico. *J Geophys Res Earth Surf* 121:128–145. <https://doi.org/10.1002/2014JF003421>. Received
- Salio P, Nicolini M, Saulo AC (2002) Chaco low-level jet events characterization during the austral summer season. *J Geophys Res Atmos* 107:4816. <https://doi.org/10.1029/2001JD001315>
- Schwerdtfeger W (1976) *Climates of Central and South America*. World Surv. Climatol., vol 12. Elsevier Sci., New York
- Segura H, Junquas C, Espinoza JC et al (2019) New insights into the rainfall variability in the tropical Andes on seasonal and interannual time scales. *Climate Dyn* 53:405–426. <https://doi.org/10.1007/s00382-018-4590-8>
- Segura H, Espinoza JC, Junquas C et al (2020) Recent changes in the precipitation-driving processes over the southern tropical Andes/western Amazon. *Climate Dyn*. <https://doi.org/10.1007/s00382-020-05132-6>
- Seiler C, Hutjes RWA, Kabat P (2013) Climate variability and trends in Bolivia. *J Appl Meteorol Climatol* 52:130–146. <https://doi.org/10.1175/JAMC-D-12-0105.1>
- Seluchi ME, Marengo JA (2000) Tropical—midlatitude exchange of air masses during summer and winter in South America: climatic aspects. *Int J Climatol* 1190:1167–1190
- Seluchi ME, Saulo AC, Nicolini M, Satyamurty P (2003) The North-western Argentinean low: a study of two typical events. *Mon Weather Rev* 131:2361–2378. [https://doi.org/10.1175/1520-0493\(2003\)131<2361:TNALAS>2.0.CO;2](https://doi.org/10.1175/1520-0493(2003)131<2361:TNALAS>2.0.CO;2)
- Sicart JE, Espinoza JC, Quéno L et al (2016) Radiative properties of clouds over a tropical Bolivian glacier: seasonal variations and relationship with regional atmospheric circulation. *Int J Climatol* 36:3116–3128. <https://doi.org/10.1002/joc.4540>
- Solman SA, Sanchez E, Samuelsson P et al (2013) Evaluation of an ensemble of regional climate model simulations over South America driven by the ERA-Interim reanalysis: model performance and uncertainties. *Climate Dyn* 41:1139–1157. <https://doi.org/10.1007/s00382-013-1667-2>
- Strecker MR, Alonso RN, Bookhagen B et al (2007) Tectonics and climate of the Southern Central Andes. *Annu Rev Earth Planet Sci* 35:747–787. <https://doi.org/10.1146/annurev.earth.35.031306.140158>
- Sulca J, Takahashi K, Espinoza JC et al (2018) Impacts of different ENSO flavors and tropical Pacific convection variability (ITCZ, SPCZ) on austral summer rainfall in South America, with a focus on Peru. *Int J Climatol* 38:420–435. <https://doi.org/10.1002/joc.5185>
- Thompson LG, Mosley-Thompson E, Bolzan JF et al (1985) A 1500-year record of tropical precipitation in ice cores from the Quelccaya Ice Cap, Peru. *Science* 229:971–973
- Turcotte DL, Greene L (1993) A scale-invariant approach to flood-frequency analysis. *Stoch Hydrol Hydraul* 7:33–40. <https://doi.org/10.1007/BF01581565>
- Vera CS, Vigliarolo PK (2002) A diagnostic study of cold-air outbreaks over South America. *Mon Weather Rev* 128:3–24. [https://doi.org/10.1175/1520-0493\(2000\)128<0003:adsoca>2.0.co;2](https://doi.org/10.1175/1520-0493(2000)128<0003:adsoca>2.0.co;2)
- Vera C, Higgins W, Amador J et al (2006) Toward a unified view of the American monsoon systems. *J Climate* 19:4977–5000
- Vuille M, Keimig F (2004) Interannual variability of summertime convective cloudiness and precipitation in the Central Andes derived from ISCCP-B3 data. *J Climate* 17:3334–3348
- Vuille M, Bradley R, Keimig F (2000) Interannual climate variability in the Central Andes and its relation to tropical Pacific and Atlantic forcing. *J Geophys Res* 105:12447–12460. [https://doi.org/10.1175/1520-0442\(2000\)013<2520:CVITAO>2.0.CO;2](https://doi.org/10.1175/1520-0442(2000)013<2520:CVITAO>2.0.CO;2)
- Wang XY, Li X, Zhu J et al (2018) The strengthening of Amazonian precipitation during the wet season driven by tropical sea surface temperature forcing. *Environ Res Lett* 13:094015. <https://doi.org/10.1088/1748-9326/aadbb9>
- Wolman M, Miller J (1960) Magnitude and frequency of forces in geomorphic processes. *J Geol* 68:54–74
- Ye S, Li H, Huang M et al (2014) Regionalization of subsurface storm-flow parameters of hydrologic models: derivation from regional analysis of streamflow recession curves. *J Hydrol* 519:670–682. <https://doi.org/10.1016/j.jhydrol.2014.07.017>
- Zhou J, Lau K-M (1998) Does a monsoon climate exist over South America? *J Climate* 11:1020–1040

**Publisher's Note** Springer Nature remains neutral with regard to jurisdictional claims in published maps and institutional affiliations.